Radiation of a pulsating portion of a sphere: application to horn radiation

Thomas Hélie and Xavier Rodet

Running title: Radiation of a pulsating portion of a sphere

Thomas Hélie

Ircam-CNRS, Equipe analyse-synthèse, 1 place Igor Stravinsky, 75004, Paris, France

Tel: 01.44.78.15.71

Fax: 01.44.78.15.40

Thomas.Helie@ircam.fr

Xavier Rodet

Ircam-CNRS, Equipe analyse-synthèse, 1 place Igor Stravinsky, 75004, Paris, France

Tel: 01.44.78.48.68

Fax: 01.44.78.15.40

Xavier.Rodet@ircam.fr

last revised: 05 December 2002

50 pages submitted, 5 Tables, and 14 Figures.

Abstract

This paper introduces the modeling of the radiation of a sphere, part of which, $\mathcal{S}_0$, is pulsating with an uniform velocity while the other remains motionless. Velocity and pressure can be expressed analytically in the space outside the sphere using spherical harmonic decomposition. The radiation impedance can then be deduced, providing a model approximating the radiation of horns, accounting for the curvature of the wavefront. The angular dependence of the radiation impedance is eliminated by averaging on $\mathcal{S}_0$ to remain compatible with most of simplified models of horns whose equations depend on a unique space variable. This averaging provides an analytical expression representing the optimal approximation, minimizing the mean square error. Three simple parametric models, which are inexpensive to simulate and approximate this model of impedance with various precisions, are proposed. They are well adapted to real-time applications, such as the simulation of wind instruments. Their parameters are given according to the geometrical characteristics of $\mathcal{S}_0$ and the stability is checked. The error introduced by these models is negligible compared to the original due to averaging on $\mathcal{S}_0$.

PACS numbers: 43-20, 43-75.

List of symbols

p	acoustic pressure
v	particle acoustic velocity
ρ_0	density of the air
c_0	speed of sound in the air
$Z_c = \rho_0 c_0$	characteristic specific impedance
$\mathbf{e_r}$	radial vector
$\mathcal{S}$	radiant sphere
$\mathcal{S}_0 \subset \mathcal{S}$	pulsating portion of the sphere $\mathcal{S}$
r_0	radius of the sphere $\mathcal{S}$
θ_0	angle associated with $\mathcal{S}_0$
$\langle . \rangle_{\mathcal{S}_0}$	average operator on $\mathcal{S}_0$
$\mathbf{1}_{[0,\theta_0]}(\theta)$	$= 1$ if $0 \leq \theta \leq \theta_0$
	$= 0$ if not
$\mathbb{P}_n(x)$	Legendre polynomials
$h_n(z)$	outgoing spherical Hankel functions
$\mathrm{o}(z^p)$	function negligible in comparison to z^p
C_n^k	binomial coefficient
$\triangleq$	definition of an expression
$f(z) \underset{0}{=}$	$f(z)$ equals for z in the vincinity of 0

1 Introduction

The shape of a horn has a strong influence on the acoustic wave propagation. This is one of the reasons why the acoustic modeling of pipes with varying cross-sections has been extensively investigated, witnessed by the large bibliography compiled by Eisner [1] on the "Webster's equation". The ongoing interest in this equation, derived in the 18th century by Bernoulli [2] and Lagrange [3], follows from the fact that this model has a one-dimensional space dependence. The space dimensionality goes hand in hand with algorithmic complexity, as can be observed in the higher cost modal decomposition used by Cho [4] versus the lower cost one used by Berners [5]. The eigenfunctions used by Cho to give the rigorous solution of hyperbolic horns have a two dimensional dependence, whereas the ones used by Berners to solve the Sturm-Liouville problem related to the Webster's equation have only one.

The Webster's model contains an ambiguity, however. It can be computed from different and non-equivalent assumptions about the wavefront geometry, and has been often computed assuming planar waves. Authors such as Lambert [6] or Weibel [7] reported the inadequacy of this planar wave assumption, and postulated spherical one. The quasi-sphericity of wavefronts was experimentally established in the low frequency range and carefully studied by Benade and Jansson [8, 9].

The same ambiguity effects the radiation impedances used in modelings of pipes based on one-dimensional propagation equations. The most widely used impedances are those of a baffled planar piston [10], an unflanged circular pipe [11], an unbaffled planar piston [12], and a flanged circular pipe [13], for which planar waves are assumed as a good approximation.

As a matter of fact, these models are extensively used in modelings of musical instruments: the Rayleigh's model for an oboe [14], the Levine's model for a brass [15], etc... The difference between piston and pipe models is the awareness of evanescent modes. Caussé, Kergomard, and Lurton [15] have introduced a correction for the case of spherical

waves, normalizing the impedance by the ratio A_p/A_s where A_p and A_s are respectively the planar and spherical areas. This result was later used by Scavone [16]. However, this constant ratio does not account for effects due to the curvature of the wavefront, such as modifications of resonance features or phase. Thus, when the angle θ_0 of the tangent cone at the horn output (see Fig. 1) is not small, the curvature is important and these effects should be taken into account.

In order to obtain a more adequate geometric model for which rigorous analytical expressions can be derived, we propose to (see Fig. 1):

(i) assimilate the true wave velocity with the velocity of a pulsating portion $\mathcal{S}_0$ of a sphere $\mathcal{S}$ inscribed in the tangent cone at the horn output,

(ii) assimilate the rigid walls of the pipe with the other portion of the sphere $\mathcal{S} - \mathcal{S}_0$ which is assumed to be motionless.

[Fig. 1 about here]

The assumption (i) makes possible a correct approximation of the shape of the wavefront. The assumption (ii) proposes a geometry rather distant from that of the horn, but allows the rigorous derivation of analytical equations. It preserves the concept of the inside and the outside of the pipe, and keeps a realistic spatial filling. More importantly, the model derived by Levine [11] is validated "throughout the wavelength range of dominant mode (planar wave) propagation", and as a result this model is valid over a comparable range. Because of the geometric error induced by (ii), this range corresponds to large wavelengths with regards to the radius of $\mathcal{S}$, noted r_0. This approximation remains valid near the axis of symmetry for small wavelengths with regards to r_0. This can be qualitatively justified because the effect of diffraction is weak and the phenomenon of the acoustic shadow dominant. Additional model simplifications are often needed to be well adapted to time-domain simulation. For example, Doutaut, Matignon, and Chaigne [17] have chosen to approximate Rayleigh's impedance as well as Levine's because of such

practical considerations. They approach both impedances with second order linear differential systems. In this paper, similar approximated models are designed in the class of linear differential systems with delay.

The structure of the paper is the following: section 2 establishes exact analytical expressions, and studies the impedance function with respect to

the dependence on physical constants (ρ_0 and c_0) and on the radius r_0,

the asymptotic behaviour versus frequency,

the influence of the angle θ_0.

The asymptotic study shows that at first approximation the impedance is comparable to a first order high-pass transfer function as commonly observed for the radiation of pipes. In Sec. 3, the analytical expression of the average of the impedance on the portion of a sphere $\mathcal{S}_0$ is derived. The averaging approximation comparable to that of Rayleigh or Levine is justified and errors are estimated. It leads to the angular independent quantity which minimizes the mean square error. Sec. 4 defines three simplified models which approach more and more closely the average impedance. As mentioned above, these models are sought in the class of differential systems with delay, adapted to time-domain simulation. Their parameters are estimated in order to obtain the best approximation of the average impedance, and are given according to r_0, θ_0, ρ_0, and c_0. Additonal errors are quantified. A comparative study is then summarized in a diagram outlining the traddeoffs between precision and complexity in the three models. Finally, the dynamical systems associated with both impedance and admittance models are given and their stability is checked.

2 Radiation of a portion of a sphere

2.1 Basis of decomposition and analytical expressions

Let $\mathcal{S}$ be a sphere the surface of which is animated by a radial velocity expressed in Fourier's domain by $v_{\mathcal{S}}(\theta,f)\,\mathrm{e}^{i2\pi ft}\,\mathbf{e_r}$. The amplitude of this velocity can be decomposed on the basis of Legendre polynomials

$$v_{\mathcal{S}}(\theta,f)=\sum_{n=0}^{+\infty}V_n(f)\;\mathbb{P}_n(\cos\theta) \tag{1}$$

where

$$V_n(f)=\frac{2n+1}{2}\int_0^{\pi}v_{\mathcal{S}}(\theta,f)\,\mathbb{P}_n(\cos\theta)\;\sin\theta\;\mathrm{d}\theta. \tag{2}$$

Under the assumption of linear dissipationless acoustics, the pressure radiated in external space ($r\geq r_0$) takes the form [10, 18]

$$p(r,\theta,f)\,\mathrm{e}^{i2\pi ft}=-iZ_c\sum_{n=0}^{+\infty}\frac{h_n\left(\frac{2\pi f\,r}{c_0}\right)}{h_n{}'\left(\frac{2\pi f\,r_0}{c_0}\right)}\,V_n(f)\,\mathbb{P}_n(\cos\theta)\,\mathrm{e}^{i2\pi ft}. \tag{3}$$

h_n represent the outgouing spherical Hankel functions. $Z_c=\rho_0c_0$ is the characteristic specific impedance.

These results make possible the calculation of the radiated pressure for the problem determined by (i) and (ii). The coefficients $V_n(f,\theta_0)$ are deduced from Eq. (2) taking $v_{\mathcal{S}}(\theta,f)=v_0(f)\,\mathbf{1}_{[0,\theta_0]}(\theta)$ by $\forall n\in\mathbb{N}$,

$$V_n(\theta_0,f)=v_0(f)\,\mu_n(\theta_0) \tag{4}$$

where

$$\mu_n(\theta_0)\triangleq\frac{\mathbb{P}_{n-1}(\cos\theta_0)-\mathbb{P}_{n+1}(\cos\theta_0)}{2} \tag{5}$$

with the convention $\mathbb{P}_{-1}(X)=1$, and where $\mathbf{1}_{[0,\theta_0]}(\theta)=1$ if $\theta\in[0,\theta_0]$ and $\mathbf{1}_{[0,\theta_0]}(\theta)=0$ if not.

The transfer function $H_{\mathcal{S}_0}(r,\theta,f) \triangleq p(r,\theta,f)/v_0(f)$ between the velocity of $\mathcal{S}_0$ and the pressure in a point of the external space is given by

$$H_{\mathcal{S}_0}(f,r,\theta) = -iZ_c \sum_{n=0}^{+\infty} \frac{h_n\left(\frac{2\pi f\, r}{c_0}\right)}{h_n{}'\left(\frac{2\pi f\, r_0}{c_0}\right)} \mu_n(\theta_0)\, \mathbb{P}_n(\cos\theta). \tag{6}$$

The specific impedance on $\mathcal{S}_0$ is

$$Z_{\mathcal{S}_0}(f,\theta) \triangleq H_{\mathcal{S}_0}(f,r_0,\theta). \tag{7}$$

2.2 Dependence of the impedance on ρ_0, c_0 and r_0

Considering the non-dimensional variables $\lambda \triangleq r/r_0$ and $\nu \triangleq r_0 f/c_0$, and normalizing $H_{\mathcal{S}_0}$ by the characteristic specific impedance Z_c leads to the definition of the normalized transfer function

$$\mathcal{H}_{\theta_0}(\nu,\lambda,\theta) = -i \sum_{n=0}^{+\infty} \mu_n(\theta_0)\, \mathbb{P}_n(\cos\theta)\, \frac{h_n(2\pi\nu\,\lambda)}{h_n{}'(2\pi\nu)} \tag{8}$$

from which $H_{\mathcal{S}_0}(f,r,\theta)$ is straighforwardly deduced by

$$H_{\mathcal{S}_0}(f,r,\theta) \;=\; Z_c \;\mathcal{H}_{\theta_0}\left(\frac{r_0}{c_0}f, \frac{r}{r_0}, \theta\right). \tag{9}$$

The normalized wavenumber $2\pi\nu$ which appears in Eq. (8) is kr_0 where k is the acoustic wavenumber.

For $\lambda = 1$, the normalized specific impedance on $\mathcal{S}_0$ is obtained

$$\mathcal{Z}_{\theta_0}(\nu,\theta) \triangleq -i \sum_{n=0}^{+\infty} \mu_n(\theta_0)\, \mathbb{P}_n(\cos\theta)\, \gamma_n(2\pi\nu) \tag{10}$$

where

$$\gamma_n(z) \triangleq \frac{h_n(z)}{h_n{}'(z)}. \tag{11}$$

In the following sections, these quantities are used because of their independence from physical constants and the radius r_0.

2.3 Asymptotic study of the normalized impedance versus frequency

From [19] (see equations (10.1.17) and (10.1.24)), it follows that

$$h_n(z) = i^{n+1}\frac{e^{-iz}}{z}\sum_{k=0}^{n} C_{n+\frac{1}{2}}^k (2iz)^{-k} \tag{12}$$

and

$$h_n{}'(z) = \frac{n}{z}h_n(z) - h_{n+1}(z) \tag{13}$$

where C_n^k are the binomial coefficients. γ_n takes the simpler form

$$\gamma_n(z) = \left[\frac{n}{z} - i\frac{\sum_{k=0}^{n+1} C_{n+\frac{3}{2}}^k (2iz)^{-k}}{\sum_{k=0}^{n} C_{n+\frac{1}{2}}^k (2iz)^{-k}}\right]^{-1}. \tag{14}$$

The asymptotic expansion of γ_n for $z \to 0$ is written as follows

$$\begin{aligned}\gamma_n(z) &\underset{0}{=} \left[n - \frac{C_{n+\frac{3}{2}}^{n+1}}{2C_{n+\frac{1}{2}}^n}\right]^{-1} z + \mathrm{o}(z)\\ &\underset{0}{=} \frac{4(n+1)}{4n^2+2n-3}z + \mathrm{o}(z).\end{aligned} \tag{15}$$

This result shows that at low frequencies and for each mode n, $\mathcal{Z}_{\theta_0}$ has the behaviour of a first order derivation operator. Under the assumption of the convergence of the series, the expansion takes the form for $\theta \in [0, \theta_0]$

$$\mathcal{Z}_{\theta_0}(\nu,\theta) \underset{0}{=} 8i\pi\nu\sum_{n=0}^{+\infty}\frac{(n+1)\mu_n(\theta_0)}{4n^2+2n-3}\mathbb{P}_n(\cos\theta) + \mathrm{o}(\nu). \tag{16}$$

The same expansion for $\frac{1}{z} \to 0^+$ is written

$$\gamma_n\left(\frac{1}{z}\right) \underset{0^+}{=} \left[-i\frac{\sum_{k=0}^{n+1} C_{n+\frac{3}{2}}^0}{\sum_{k=0}^{n} C_{n+\frac{1}{2}}^0}\right]^{-1} + \mathrm{o}(1) \underset{0^+}{=} i + \mathrm{o}(1). \tag{17}$$

Thus, at high frequencies and for each mode n, $\mathcal{Z}_{\theta_0}$ has the behaviour of a multiplicative gain. Under the assumption of the convergence of the series, the expansion takes the form for $\theta \in [0, \theta_0]$,

$$\mathcal{Z}_{\theta_0}(\nu, \theta) \underset{\nu^{-1} \to 0^+}{=} \mathbf{1}_{[0,\theta_0]}(\theta) + \mathrm{o}(1). \tag{18}$$

2.4 Dependence of the impedance on θ and θ_0

An exact study of the dependence of $\mathcal{H}_{\theta_0}$ on (θ, θ_0) is difficult. The study is therefore restricted here to the numerical study of $\mathcal{Z}_{\theta_0}(\nu, \theta)$. The results presented below are obtained for $\theta_0 \in \{30°; 70°\}$, $\theta \in [0°, 100°]$ and $\nu \in [0, 10]$, and the calculations are made for a finite number of modes $n \in [0, N]_{\mathbb{N}}$ with $N = 300$.

The effect of the truncation of the n modes on velocity $v_{\mathcal{S}}$ is highlighted by Fig. 2 (a) (b) which represents $\sum_{n=0}^{N} \mu_n(\theta_0)\, \mathbb{P}_n(\cos\theta) \approx \frac{v_{\mathcal{S}}}{v_0}(\theta)$.

In Fig. 2 (c) (d), the modulus of the adimensional quantity $p_{\mathcal{S}}(\theta, \nu)/(Z_c\, v_0(\nu))$ is represented for the same angles θ_0. Note that $\forall \nu \in \mathbb{R}$ and $\forall \theta \in [0, \theta_0]$, $p_{\mathcal{S}}(\theta, \nu)/(Z_c\, v_0(\nu)) = \mathcal{Z}_{\theta_0}(\nu, \theta)$. Figures 2 (c) (d), show the strong attenuation of p on $\mathcal{S} - \mathcal{S}_0$, the asymptotic behaviour at low frequencies, and the dependence on θ.

[Figure 2 about here]

3 Impedance averaged on the portion $\mathcal{S}_0$ of the sphere $\mathcal{S}$

In many simplified contexts, models of pipes present a space dependence on one variable only, most often the X-coordinate along the axis of the pipe. This is the case for waveguide modeling [16] or for any other one-dimensional modeling such as the Webster's equation [5].

To connect a radiation impedance to the end of such a model, it is necessary that this

impedance does not depend on other space variables. In the present paper, the normalized specific impedance $\mathcal{Z}_{\theta_0}(\nu,\theta)$ must be approximated by a quantity independent of the angle θ. It is proposed here to average the impedance on $\mathcal{S}_0$.

3.1 Average operator

The average operator on $\mathcal{S}_0$ is defined as follows

$$f \mapsto \langle f \rangle_{s_0} = \frac{\int_0^{\theta_0} f(\theta)\sin\theta\,\mathrm{d}\theta}{1-\cos\theta_0}. \tag{19}$$

A remarkable property is that $\langle f \rangle_{s_0}$ is the θ-independent quantity F which minimizes the mean square error $\langle |f-F|^2 \rangle_{s_0}$. This result comes from the fact that $(f,g) \mapsto \langle f g^* \rangle_{s_0}$ is a scalar product on the space of the functions continuous in $\theta \in [0,\theta_0]$, and that $\langle f \rangle_{s_0}$ is the orthogonal projection of f on the subspace of the functions independent of θ.

3.2 Analytical expression

The application of the linear operator $\langle . \rangle_{s_0}$ on Eq. (8) gives, after evaluation for $\lambda = 1$,

$$\langle \mathcal{Z}_{\theta_0} \rangle_{s_0}(\nu) = -i \sum_{n=0}^{+\infty} \mu_n(\theta_0) \langle \mathbb{P}_n(\cos\theta) \rangle_{s_0} \gamma_n(2\pi\nu). \tag{20}$$

According to Eq. (2) and Eq. (4),

$$\langle \mathbb{P}_n(\cos\theta) \rangle_{s_0} = \frac{2}{1-\cos\theta_0} \frac{\mu_n(\theta_0)}{2n+1}. \tag{21}$$

Finally, the following analytical expression is obtained by

$$\langle \mathcal{Z}_{\theta_0} \rangle_{s_0}(\nu) = \frac{-2i}{1-\cos\theta_0} \sum_{n=0}^{+\infty} \frac{[\mu_n(\theta_0)]^2}{2n+1} \gamma_n(2\pi\nu) \tag{22}$$

and the result of its computation (still for $N = 300$) is presented in Fig. 3 (a) (b). $\langle Z_{\mathcal{S}_0} \rangle_{s_0}(f)$ is easily obtained by

$$\langle Z_{\mathcal{S}_0} \rangle_{s_0}(f) = Z_c \ \langle \mathcal{Z}_{\theta_0} \rangle_{s_0}\left(\frac{r_0}{c_0} f\right). \tag{23}$$

[Figure 3 about here]

3.3 Quantification of errors

The mean square error made on $\mathcal{Z}_{\theta_0}$ is

$$\mathcal{E}_0(\theta_0,\nu) \triangleq \left\langle \left| \mathcal{Z}_{\theta_0} - \langle \mathcal{Z}_{\theta_0} \rangle_{\mathcal{S}_0} \right|^2 \right\rangle_{\mathcal{S}_0} (\nu). \tag{24}$$

This error (computed for the first modes $0 \leq n \leq N$) is represented on Fig. 3 (c). It is decreasing with the angle θ_0, and is less than 10^{-1} for all ν when $\theta_0 > 50°$. This is still the case for the relative error $\mathcal{E}_0(\theta_0,\nu)/\left\langle |\mathcal{Z}_{\theta_0}|^2 \right\rangle_{\mathcal{S}_0}(\nu)$ so that $\langle \mathcal{Z}_{\theta_0} \rangle_{\mathcal{S}_0}(\nu)$ is a satisfactory approximation of $\mathcal{Z}_{\theta_0}(\nu,\theta)$ over the complete frequency range, for large angles $\theta_0 > 50°$.

The normalized frequency for which this square error is maximum is graphically estimated to $\nu^* \approx \frac{0.58}{\theta_0}$, where θ_0 is in radians. For example, acoustic measurements on a Blessing trumpet [20] show that the bore behaves as a resonator at frequencies $f < 1600$Hz corresponding to $\nu < 0.3$ whereas $\nu^* \approx 0.6$. Therefore, the internal resonance frequencies are not in the vicinity of the maximal error zone, so the averaged specific impedance model can be used to represent and study the internal behaviour of the instrument.

4 Simplified models of impedance

The analytical expression Eq. (22) is adapted to the modeling of resonators depending on a unique space variable, but remains too complicated for time-domain simulation: the functions γ_n correspond to complicated time operators costly to implement. Three parametrized models $\mathcal{M}_k^{(\mathbf{p}(\theta_0))}(\nu)$ $(k = 1, 2, 3)$which approximate $\langle \mathcal{Z}_{\theta_0} \rangle_{\mathcal{S}_0}(\nu)$ are now presented. According to the initial goal, they all belong to the class of the differential systems with delay [21].

The parameters $\mathbf{p}(\theta_0)$ are estimated by minimizing the criterion defined by the average on $\nu \in [0, +\infty]$ of the mean square error on $\mathcal{S}_0$

$$\mathcal{E}_k(\theta_0,\nu) = \left\langle \left| \mathcal{Z}_{\theta_0} - \mathcal{M}_k^{(\mathbf{p}(\theta_0))} \right|^2 \right\rangle_{\mathcal{S}_0} (\nu) \tag{25}$$

or equivalently, of the mean cumulated error

$$\Delta\mathcal{E}_k(\theta_0,\nu) \triangleq \mathcal{E}_k(\theta_0,\nu) - \mathcal{E}_0(\theta_0,\nu) = \left|\langle\mathcal{Z}_{\theta_0}\rangle_{S_0}(\nu) - \mathcal{M}_k^{(\mathbf{p}(\theta_0))}(\nu)\right|^2. \tag{26}$$

These two quantities lead to exactly the same optimum but the second one does not require the application of $\langle.\rangle_{S_0}$ for each minimization.

In practice, the criterion built on $\Delta\mathcal{E}_k$ is numerically approximated by

$$\mathcal{C}_k(\mathbf{p}(\theta_0)) \triangleq \frac{1}{L\delta_\nu}\sum_{l=0}^{L-1}\left|\frac{-2i}{1-\cos\theta_0}\sum_{n=0}^{N}\frac{\mu_n(\theta_0)^2}{2n+1}\,\gamma_n(2\pi\nu_l) - \mathcal{M}_k^{(\mathbf{p}(\theta_0))}(\nu_l)\right|^2 \tag{27}$$

for $N=300$, $\nu_l = \nu_{min} + l\,\delta_\nu \;\; \forall l \in [0, L-1]_{\mathbb{N}}$, $\delta_\nu = \frac{\nu_{max}-\nu_{min}}{L-1}$, $\nu_{min} = 10^{-3}$, $\nu_{max} = 10$, and $L = 400$. Usually, this choice largely covers the range of audio frequencies. For the same Blessing trumpet [20], with $c_0 = 340\text{m.s}^{-1}$, the range goes from 5Hz to 52kHz.

In the following, the results are given for θ_0 increasing from 10° to 90° with a step of 2°.

4.1 First order high-pass model

The simplest model presented here reproduces the asymptotic behaviour of $\langle\mathcal{Z}_{\theta_0}\rangle_{S_0}(\nu)$, i.e. the one of a first order high-pass transfer function, with a unitary limit gain at high frequencies

$$\mathcal{M}_1^{(\nu_c)}(\nu) \triangleq \frac{i\nu/\nu_c}{1+i\nu/\nu_c}. \tag{28}$$

Parameter ν_c represents the cut-off frequency, and must be estimated for each θ_0.

The estimation of ν_c could be carried out on the asymptote of $\langle\mathcal{Z}_{\theta_0}\rangle_{S_0}(\nu)$ at low frequencies using Eq. (16). However, it is preferable to minimize $\mathcal{C}_1(\nu_c)$ which ensures the required optimization. This minimization is computed using the MATLAB© function `fminbnd` [22, 23] . The convergence of the algorithm leads successfully to the optimal parameters $\nu_{c\,opt}(\theta_0)$, represented on Fig. 4.

[Figure 4 about here]

The model $\mathcal{M}_1^{(\nu_c(\theta_0))}(\nu)$ obtained for these values (see Fig. 5 (a) (b)) gives a good approximation for large angles θ_0. This can be observed on the Fig. 5 (c) which represents the quadratic error $\Delta\mathcal{E}_1(\theta_0,\nu)$. Remember that $\Delta\mathcal{E}_1$ is added to the averaging error $\mathcal{E}_0$ to give the total error $\mathcal{E}_1$. Figures 3 (c) and 5 (c) show that $\forall\nu,\ \theta_0,\ \ \Delta\mathcal{E}_1 \ll \mathcal{E}_0$.

[Figure 5 about here]

A polynomial has been found

$$\mathcal{P}(X) = -0{,}4343X^4 + 2{,}321X^3 - 5{,}251X^2 + 7{,}182X + 2{,}914\,10^{-3} \tag{29}$$

which gives an approximate value of the optimum for $\theta_0 \in [10°, 90°]$

$$\nu_{capprox}(\theta_0) = 1 \,/\, \mathcal{P}(\pi\,\theta_0/180) \tag{30}$$

with a relative error less than 10^{-3}. Furthermore, the relative error introduced on $\mathcal{M}_1$ by this approximation of ν_c is $\forall\theta_0,\nu,\ \left|\frac{\mathcal{M}_1^{(\nu_{copt})} - \mathcal{M}_1^{(\nu_{capprox})}}{\mathcal{M}_1^{(\nu_{copt})}}\right| < 10^{-3}$.

4.2 Second order high-pass model

For small angles θ_0, a second order high-pass model gives a better represention of $\langle\mathcal{Z}_{\theta_0}\rangle_{s_0}$ since it can exhibit a resonance. Because of the unitary limit gain of $\langle\mathcal{Z}_{\theta_0}\rangle_{s_0}(\nu)$ at high frequencies, this model has again a particular form

$$\mathcal{M}_2^{(\alpha,\xi,\nu_c)}(\nu) \triangleq \frac{\alpha i\frac{\nu}{\nu_c} - \left(\frac{\nu}{\nu_c}\right)^2}{1 + 2i\xi\frac{\nu}{\nu_c} - \left(\frac{\nu}{\nu_c}\right)^2}. \tag{31}$$

The optimization of the parameter values (α,ξ,ν_c) is obtained by minimizing the criterion $\mathcal{C}_2(\alpha,\xi,\nu_c)$ with the MATLAB© function `fminsearch` [24, 25] which performs the local minimization of a function of several variables. The goodness of the global optimum is conditioned by the quality of initialization. Initialization is thus carefully selected. For the smallest angle $\theta_0 = 10°$, the initialization parameters are analytically derived so that the asymptotic behaviour of $\mathcal{M}_2$ at low frequencies, and its resonance parameters (frequency, modulus, and phase) are identical to those of $\langle\mathcal{Z}_{\theta_0}\rangle_{s_0}$ (see Fig. 6).

For the following optimizations, the continuity of both $\mathcal{M}_2^{(\alpha,\xi,\nu_c)}(\nu)$ and $\langle\mathcal{Z}_{\theta_0}\rangle_{s_0}$ in θ_0 is taken advantage of. This is done for successively larger θ_0 values by initializing the parameters α, ξ, and ν_c with the optimal values from the previous step in the optimization algorithm.

[Figure 6 about here]

The convergence of the algorithm leads to the satisfactory optimal parametric values represented on Fig. 7.

[Figure 7 about here]

The improvement obtained with $\mathcal{M}_2$ (see Fig. 8 (a) (b)) over $\mathcal{M}_1$ is significant since almost an order of magnitude is gained from $\Delta\mathcal{E}_1$ to $\Delta\mathcal{E}_2$ (see Fig. 8 (c)).

[Figure 8 about here]

The optimal parameter values can be approached with a relative error less than 10^{-3} for $\theta_0 \in [10°, 90°]$ by

$$\alpha(\theta_0) = 1 \,/\, \mathcal{P}_\alpha(\pi\,\theta_0/180) \tag{32}$$

$$\xi(\theta_0) = \mathcal{P}_\xi(\pi\,\theta_0/180) \tag{33}$$

$$\nu_c(\theta_0) = 1 \,/\, \mathcal{P}_{\nu_c}(\pi\,\theta_0/180) \tag{34}$$

where $\mathcal{P}_\alpha(X)$, $\mathcal{P}_\xi(X)$ and $\mathcal{P}_{\nu_c}(X)$ are low order polynomials, the coefficients of which are given in Appendix A. The relative error introduced on $\mathcal{M}_2$ by these approximations of α, ξ and ν_c is less than 10^{-3}.

This second order model is satisfactory for large angles ($\theta_0 > 60°$) but the resonances associated with $\langle\mathcal{Z}_{\theta_0}\rangle_{s_0}$ are still poorly represented for smaller angles. To cope with this problem, rather than continuing to increase the model order, a model with a delay is prefered. This choice keeps a low cost for time-domain simulation and is well adapted to $\langle\mathcal{Z}_{\theta_0}\rangle_{s_0}$ which has nearly harmonic resonances.

4.3 Model with a delay

Since the average shape of $\langle \mathcal{Z}_{\theta_0} \rangle_{S_0}$ may be represented by $\mathcal{M}_2$, an attractive improvement which seems adequate is to multiply it by a factor close to unity and representing weak resonances. These resonances must be nearly harmonic and with an amplitude decreasing with ν. Such a factor is given by $1 + \frac{\beta \mathrm{e}^{-2i\pi\frac{\nu}{\nu_\tau}}}{1+i\frac{\nu}{\nu_d}}$. The third model then takes the following form

$$\mathcal{M}_3^{(\mathbf{p})}(\nu) \triangleq \frac{\alpha i\frac{\nu}{\nu_c} - \left(\frac{\nu}{\nu_c}\right)^2}{1 + 2i\xi\frac{\nu}{\nu_c} - \left(\frac{\nu}{\nu_c}\right)^2} \left[1 + \frac{\beta \mathrm{e}^{-2i\pi\frac{\nu}{\nu_\tau}}}{1+i\frac{\nu}{\nu_d}}\right] \tag{35}$$

where $\mathbf{p} = (\alpha, \xi, \nu_c, \beta, \nu_\tau, \nu_d)$.

The function `fminsearch` is again used to optimize $\mathcal{C}_3(\alpha, \xi, \nu_c, \beta, \nu_\tau, \nu_d)$. As before, the initialization of the parameters for the lowest angle $\theta_0 = 10°$ must be carefully chosen. This is made by taking the optimal parameters α, ξ and ν_c obtained for $\mathcal{M}_2$. ν_τ is determined by the harmonic periodicity of $\langle \mathcal{Z}_{\theta_0} \rangle_{S_0}$. β and ν_d are determined by using trials until obtaining a very accurate result after convergence. For larger angles, the continuity of $\mathcal{M}_3$ in θ_0 is used again. The convergence of the algorithm leads to the satisfactory optimal parameter values $\mathbf{p}$ represented on Fig. 9 (a) (b).

[Figure 9 about here]

The results obtained with $\mathcal{M}_3$ are definitely better than with $\mathcal{M}_2$ and so close to $\langle \mathcal{Z}_{\theta_0} \rangle_{S_0}$ that only the error $\Delta\mathcal{E}_3$ is represented on Fig. 10.

[Figure 10 about here]

The complete set of parameter values is given in Appendix B. The round-off of these values introduces a relative error on $\mathcal{M}_3$ lower than 10^{-3}. This last model gives a good approximation of $\langle \mathcal{Z}_{\theta_0} \rangle_{S_0}$ even for the small angles θ_0.

4.4 Discussion on the modeling errors and comparisons

For non-dissipative fluids, the conservation of the radiated energy and of the mass permits a rigorous evaluation of the real part of the radiation impedance at the low frequency limit.

The calculation leads to

$$\Re\mathrm{e}\langle\mathcal{Z}_{\theta_0}\rangle_{\mathcal{S}_0}(\nu)\underset{0}{=}\frac{1-\cos\theta_0}{2}(2\pi\nu)^2+\mathrm{o}(\nu^2). \tag{36}$$

This result was used by Caussé, Kergomard, and Lurton [15] to give a correction ratio on the Levine's impedance taking into account the spherical wave assumption. This theoretical result is used here to compare the validity of all models in the low frequency range, computing the coefficients of the second order series expansion:

$$\mathcal{M}_k(\nu)\underset{0}{=}0+i\,c_1^{(k)}\nu+c_2^{(k)}\nu^2+\mathrm{o}(\nu^2). \tag{37}$$

These coefficients are given in table I and are represented on Fig. 11.

[Fig. 11 about here]

The coefficient c_2 computed for $\langle\mathcal{Z}_{\theta_0}\rangle_{\mathcal{S}_0}$ (still with $N=300$) matches exactly with the theory. For $\mathcal{M}_1$, the relative errors on c_1 and c_2 are very large for low aperture angles. On the contrary, for $\mathcal{M}_2$, they are much smaller for low aperture angles than for large ones. This can be explained because no frequency range is favored by the optimization. For $\mathcal{M}_3$, the size of the errors observed on c_1 and c_2 validate the approximation of $\langle\mathcal{Z}_{\theta_0}\rangle_{\mathcal{S}_0}$ by $\mathcal{M}_3$. Moreover, although the improvements made on $\mathcal{M}_3$ were put into the middle and high frequencies, this model gives very good results for low frequencies as well.

To discuss and validate the choice of the criterion $\mathcal{C}_k(\mathbf{p}(\theta_0))$ given by Eq.(27), a second optimization has been computed for this criterion under the constraints that $c_1^{(k)}=c_1^{\langle\mathcal{Z}_{\theta_0}\rangle_{\mathcal{S}_0}}$ and $c_2^{(k)}=c_2^{theo}$. Because of the number of parameters, both constraints can be imposed only for $\mathcal{M}_2$ and $\mathcal{M}_3$. The associated errors $\Delta\mathcal{E}_2$ and $\Delta\mathcal{E}_3$ are given in Fig. 12 for the apertures θ_0 where the relative errors on c_1 and c_2 are maximal.

These results show that the constraints make the error decrease in the very low frequency range but make this error increase much more in the middle frequency range, particularly for large apertures θ_0. Since the additive errors $\Delta\mathcal{E}_k$ are much smaller in the

low than in the middle frequency range, the choice is made to preserve the parameters obtained for the unconstrained optimization.

Consequently, the optimum $\langle \mathcal{Z}_{\theta_0} \rangle_{S_0}$ is approximated by the models $\mathcal{M}_{k=1,2,3}^{(\mathbf{p})}$ for the parameters optimized without constraints. These models can be used in the following way:

1. For an angle θ_0 given in degrees, the model $\mathcal{M}_k^{(\mathbf{p})}$ is selected according to the approximation accepted on $\langle \mathcal{Z}_{\theta_0} \rangle_{S_0}$ by means of the diagram in Fig. 13 and Fig. 14.

2. The optimal parameters $\mathbf{p}(\theta_0)$ of the model are given by Eq. (30) for $\mathcal{M}_1$, Eq. (34) and table III for $\mathcal{M}_2$, and table IV for $\mathcal{M}_3$.

3. The radiation specific impedance is then approximated by

$$Z_{S_0}(f) \approx Z_c \, \mathcal{M}_k^{(\mathbf{p})}\left(\frac{r_0}{c_0} f\right). \tag{38}$$

[Figure 13 about here]

[Figure 14 about here]

4.5 Dynamical systems

The three models expressed above in the frequency domain correspond all to differential linear systems with delay. These low cost systems, well adapted to time-domain simulation, can be written in the unified form

$$\sum_{k=0}^{3} A_k \frac{\mathrm{d}^k p(t)}{\mathrm{d}t^k} = Z_c \left[\sum_{l=1}^{3} B_l \frac{\mathrm{d}^l v(t)}{\mathrm{d}t^l} + \sum_{n=1}^{2} C_n \frac{\mathrm{d}^n v(t-\tau)}{\mathrm{d}t^n} \right] \tag{39}$$

where coefficients A_k, B_l and C_n are given in table II with $\omega_c = 2\pi c_0 \nu_c / r_0$, $\omega_d = 2\pi c_0 \nu_d / r_0$, $\tau = r_0/(\nu_\tau c_0)$.

[Table II about here]

In the following, the BIBO (Bounded Input, Bounded Output) stability of the various dynamical systems is studied. The dynamical systems of specific impedance (i.e. controlled by $v(t)$) are all unconditionally stable. Poles of their Laplace transform $L_k(s)$ are

respectively given for the three models by

$$\begin{aligned}\mathcal{P}_1 &= \{-\omega_c\}\\ \mathcal{P}_2 &= \left\{\omega_c\left(-\xi \pm i\sqrt{(1-\xi)(1+\xi)}\right)\right\}\\ \mathcal{P}_3 &= \mathcal{P}_2 \cup \{-\omega_d\}\end{aligned}$$

with $\omega_c > 0$, $\omega_d > 0$ and $0 < \xi < 1$. Their real part are all strictly negative.

The dynamical systems of specific admittance (i.e. controlled by $p(t)$) are all limit-stable since zeros of $L_k(s)$ are given by

$$\begin{aligned}\mathcal{Z}_1 &= \{0\}\\ \mathcal{Z}_2 &= \{0, -\alpha\omega_c\}\\ \mathcal{Z}_3 &= \{0, -\alpha\omega_c\} \cup \mathcal{E}_3\end{aligned}$$

with $\mathcal{E}_3 \subset]-\infty, 0[\times i\mathbb{R}$ (see Appendix C). The root 0, responsible for the limit of stability, thus requires the system to be controlled by a pressure of zero average.

In addition, in time simulation, the decomposition of the velocity and the pressure into outgoing (+) and incoming (−) waves is often used, as well as the reflexion functions on the outlet side of the guide. For example, for a spherical wave travelling in a cone, the specific impedances of outgoing and incoming waves are given by $Z_s^{\pm} = Z_c/(\pm 1 + i\frac{c_0}{r_0\omega})$. The coefficient of reflection at the end of the cone ($r = r_0$) is then determined by

$$\begin{aligned}p^-(f) &= \mathcal{R}_k(f)\, p^+(f),\\ \mathcal{R}_k(f) &= \frac{\left(1 - \frac{c_0}{2i\pi r_0 f}\right)\mathcal{M}_k\left(\frac{r_0}{c_0}f\right) - 1}{\left(1 + \frac{c_0}{2i\pi r_0 f}\right)\mathcal{M}_k\left(\frac{r_0}{c_0}f\right) + 1}.\end{aligned}$$

The poles and zeros can be given analytically for $\mathcal{R}_1$ and $\mathcal{R}_2$ by

$$\begin{aligned}\mathcal{P}_{\mathcal{R}_1} &= \{-(\omega_c + r_0/c_0)/2\}\\ \mathcal{Z}_{\mathcal{R}_1} &= \{\}\\ \mathcal{P}_{\mathcal{R}_2} &= \{r_1, r_2\}\\ \mathcal{Z}_{\mathcal{R}_2} &= \{-\omega_c\frac{\alpha + \omega_c r_0/c_0}{1 + (2\xi - \alpha)r_0\omega_c/c_0}\}\end{aligned}$$

with $r1 + r2 = -(r_0\omega_c(2\xi + \alpha)/c_0 + 1)/2 < 0$, $r_1 r_2 = r_0\omega_c/c_0(\alpha + r_0\omega_c/c_0)/2 > 0$, and $2\xi - \alpha > 0$ (see Fig. 7).

Thus, all the poles and zeros have a strictly negative real part. As a result, the dynamical systems associated with $\mathcal{R}_1$, $\mathcal{R}_2$, $1/\mathcal{R}_1$ and $1/\mathcal{R}_2$ are unconditionally stable.

The study of the stability of $\mathcal{R}_3$ and $1/\mathcal{R}_3$ could not have been carried out analytically. In spite of the mathematical difficulties, stability can be numerically checked by computing the pole values.

5 Conclusion

Considering the radiation of a horn as a pulsating portion of a sphere allows one to derive analytical models of radiation which account for the curvature of wavefronts. The theoretical models developed in this article show that effects due to this curvature are not negligible for large apertures θ_0. In particular, averaging the specific radiation impedance models leads to simplified analytical expressions with one-dimensional space dependence which can be compared to Rayleigh or Levine impedances. For small apertures, the averaged models exhibit similar behaviours (including resonances). For large apertures where a planar wave hypothesis no longer holds, significant differences break out and resonances vanish. The absence of local maxima is observed for $\theta_0 \geq \theta^r \approx 74°$ even if inflexion points remain. This study shows the relevance of this modeling by looking at the importance of curvature.

Furthermore, the calculation of the error introduced by the averaging on the portion of the sphere shows that the quality of averaged models is better for large apertures than for small ones. Such models are a good approximation of the radiation on the complete frequency range, especially for flaring horns. In this sense, they give an interesting alternative to the normalization of the Levine formula proposed by Caussé, Kergomard, and Lurton [15].

From a practical point of view, the second simplification presented in Sec. 4 leading to the three models $\mathcal{M}_{k=1,2,3}$, can be considered as the main result of this work. These last models provide stable, time-continous, dynamical linear systems, composed of time-differential and delay operators. The added errors are negligible compared to those due to averaging. Starting from them, a low-cost discrete time-domain simulation can be derived using finite difference methods.

Finally, although this work was dedicated to the modeling of radiation impedance, it is also useful for the simulation of the acoustic pressure in a given point of external space. This can be done by exciting the transfer function $H_{\mathcal{S}_0}$ studied in Sec. 2 2.2 with the wave velocity v_0 computed for the internal dynamics. Given geometric parameters of the portion of the sphere and the coordinates of the listening point, the transfer function depends only on the frequency. Models similar to $\mathcal{M}_{k=1,2,3}$ could then be used, and their parameters estimated, to approximate this last transfer function.

APPENDIX A: Polynomial coefficients associated with the optimal parameters of $\mathcal{M}_2$

[Table III about here]

APPENDIX B: Values of the optimal parameters of $\mathcal{M}_3$

[Table IV about here]

APPENDIX C: Proof of the stability of the specific admittance associated with $\mathcal{M}_3$

The zeros induced by the delay and whose solution whole previously definite is $\mathcal{E}_3$ are $s = Xc_0/r_0$ such that

$$X + 2\pi\nu_\tau^c \left(1 + \beta e^{-X/\nu_\tau}\right) = 0 \tag{C1}$$

By posing $X = x + iy$, the real part of the equality C1 is written

$$f(x) = \cos(y/\nu_\tau) \tag{C2}$$

where

$$f(x) \triangleq \left(\frac{x}{2\pi\nu_\tau^c} + 1\right) \frac{e^{x/\nu_\tau}}{\beta} \tag{C3}$$

The study of f, continuous on $\mathbb{R}$, shows that it is strictly decreasing for $x \in]x^*, +\infty[$ on $]0, f^*[$, reached its minimum for $x = x^*$ at f^*, and is strictly increasing for $x \in]x^*, +\infty[$ on $]f^*, +\infty[$, with $x^* = -(2\pi\nu_\tau^c + \nu_\tau) < 0$ and $f^* = -\nu_\tau/\beta \exp(1 + 2\pi\nu_\tau^c/\nu_\tau) < 0$.

[Table V about here]

Thus, there is a unique x_1 such as $f(x_1) = 1$. Moreover, $f(0) = 1/\beta$ and $1/\beta > 1$ (see

Fig. 7). Consequently, $x^* < x_1 < 0$ and $\forall x > x_1,\ |f(x)| > 1$.

The function $|\cos|$ being raised by 1, it can be concluded that

$$x \in\ ]-\infty, x_1] \quad \subset\ ]-\infty, 0[\tag{C4}$$

and thus that the real part of the solutions of Eq. (C1) are all strictly negative.

Acknowledgements

The authors would like to thank Jean Kergomard and Michel Bruneau for interesting discussions about this work, as well as David Ralley for proofreading.

References

[1] E. Eisner. Complete solutions of the "Webster" horn equation. *J. Acoust. Soc. Amer.*, 41:1126–1146, 1967.

[2] D. Bernoulli. Physical, mechanical and analytical researches on sound and on the tones of differently constructed organ pipes. Mém. Acad. Sci. (Paris), 1762. (in French).

[3] J. L. Lagrange. New researches on the nature and propagation of sound. Misc. Taurinensia (Mélanges Phil. Math., Soc. Roy. Turin), 1760-1761. (in French).

[4] Y. C. Cho. Rigorous solutions for sound radiation from circular ducts with hyperbolic horns or infinite baffle. *Journal of Sound and Vibration*, 69:405–425, 1980.

[5] D. P. Berners. *Acoustics and signal processing techniques for physical modeling of brass instruments*. PhD thesis, Standford University, 1999.

[6] R. F. Lambert. Acoustical studies of the tractrix horn. I. *J. Acoust. Soc. Amer.*, 26:1024–1028, 1954.

[7] E. S. Weibel. On Webster's horn equation. *J. Acoust. Soc. Amer.*, 27:726–727, 1955.

[8] A.H. Benade and E.V. Jansson. On plane and spherical waves in horns with nonuniform flare. I. Theory of radiation, resonance frequencies, and mode conversion. *Acustica*, 31:79–98, 1974.

[9] A.H. Benade and E.V. Jansson. On plane and spherical waves in horns with nonuniform flare. II. Prediction and measurements of resonance frequencies and radiation losses. *Acustica*, 31:185–202, 1974.

[10] P. M. Morse and K. U. Ingard. *Theoretical acoustics*. McGraw-Hill, New York, 1968.

[11] H. Levine and J. Schwinger. On the radiation of sound from an unflanged circular pipe. *Physical Review*, 73:383–406, 1948.

[12] T. Nimura and Y. Watanabé. Effect of a finite circular baffle board on acoustic radiation. *J. Acoust. Soc. Amer.*, 25:76–80, 1953.

[13] A. N. Norris and I.C. Sheng. Radiation of sound from a circular pipe with an infinite flange. *J. Sound Vibration*, 135:85–93, 1989.

[14] G.R. Plitnik and W.J. Strong. Numerical method for calculating input impedances of the oboe. *J. Acoust. Soc. Amer.*, 65:816–825, 1979.

[15] R. Caussé, J. Kergomard, and X. Lurton. Input impedance of brass musical instruments - comparison between experiment and numerical models. *J. Acoust. Soc. Amer.*, 75:241–254, 1984.

[16] G. P. Scavone. *An acoustic analysis of single-reed woodwind instruments with an emphasis on design and performance issues and digital waveguide modeling techniques.* PhD thesis, Stanford University, 1997.

[17] V. Doutaut, D. Matignon, and A. Chaigne. Numerical simulations of xylophones. II. time-domain modeling of the resonator and of the radiated sound pressure. *J. Acoust. Soc. Amer.*, 104:1633–1647, 1998.

[18] Michel Bruneau. *Manuel d'acoustique fondamentale.* études en mécanique des matériaux et des structures. Hermès, Éditions HERMÈS, 8 quai du Marché-Neuf, 75004 Paris, FRANCE, 1998. p.245.

[19] Milton Abramowitz and Irene A. Stegun, editors. *Handbook of mathematical functions.* Dover publications, inc., New York, 1970.

[20] R. Caussé. Geometrical data and acoustical measurements of a blessing trumpet. internal data, 1999. Équipe acoustique instrumentale, Ircam - centre Georges Pompidou, 1 pl. Igor Stravinsky, 75004 Paris, France.

[21] J. K. Hale. *Dynamics and Delays.* in Delay Differential Equations and Dynamical Systems, Proc., 1990, S. Busenberg & M. Martelli (Eds.). Springer Verlag, 1991. Lecture Notes in Mathematics 1475.

[22] Matlab function `fminbnd`. Original coding by Duane Hanselman, University of Maine. copyright (c) 1984-98 by The MathWorks, Inc., 1998. Revision: 1.6.

[23] Forsythe, Malcolm, and Moler. *Computer Methods for Mathematical Computations.* Prentice-Hall, 1976.

[24] Matlab function `fminsearch`. Copyright (c) 1984-98 by the mathworks, inc., 1998.

[25] Jeffrey C. Lagarias, James A. Reeds, Margaret H. Wright, and Paul E. Wright. Convergence properties of the nelder-mead simplex method in low dimensions. *Society for Industrial and Applied Mathematics*, 9:112–147, 1998. http://epubs.siam.org/sambin/dbq/article/30347.

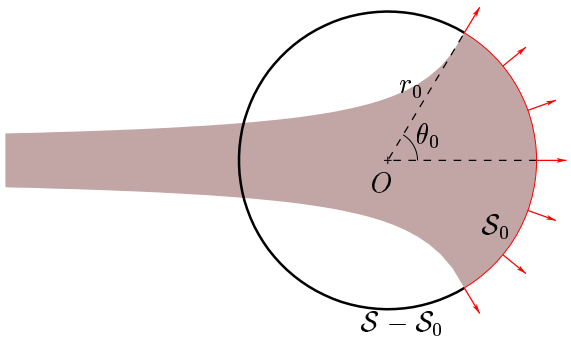

Figure 1: The radiation of the horn is approximated by that of the sphere $\mathcal{S}$, part of which, $\mathcal{S}_0$, is pulsating with an uniform velocity while the other remains motionless. The radius of $\mathcal{S}$ is noted r_0, and the angle of the tangent cone at the horn output is noted θ_0.

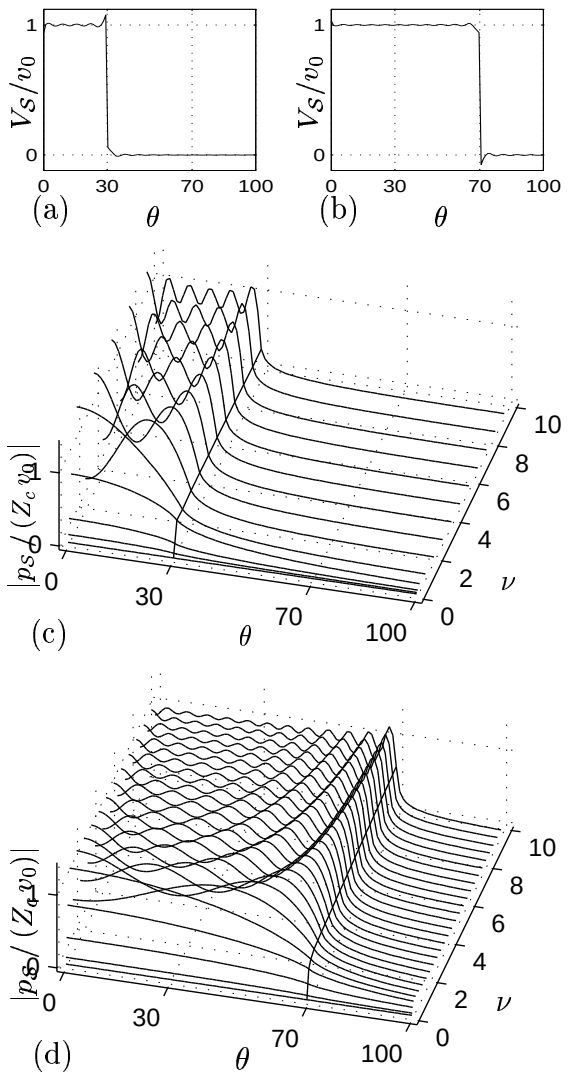

Figure 2: Approximation of the normalized velocity V_S/v_0 and the modulus of the normalized pressure in the frequency domain $p_S/(Z_c v_0)$, both computed for the first modes ($N = 300$). (a) Normalized velocity calulated with $\theta_0 = 30°$. (b) Normalized velocity calulated with $\theta = 70°$. (c) Normalized pressure calulated with $\theta = 30°$. (d) Normalized pressure calulated with $\theta = 70°$.

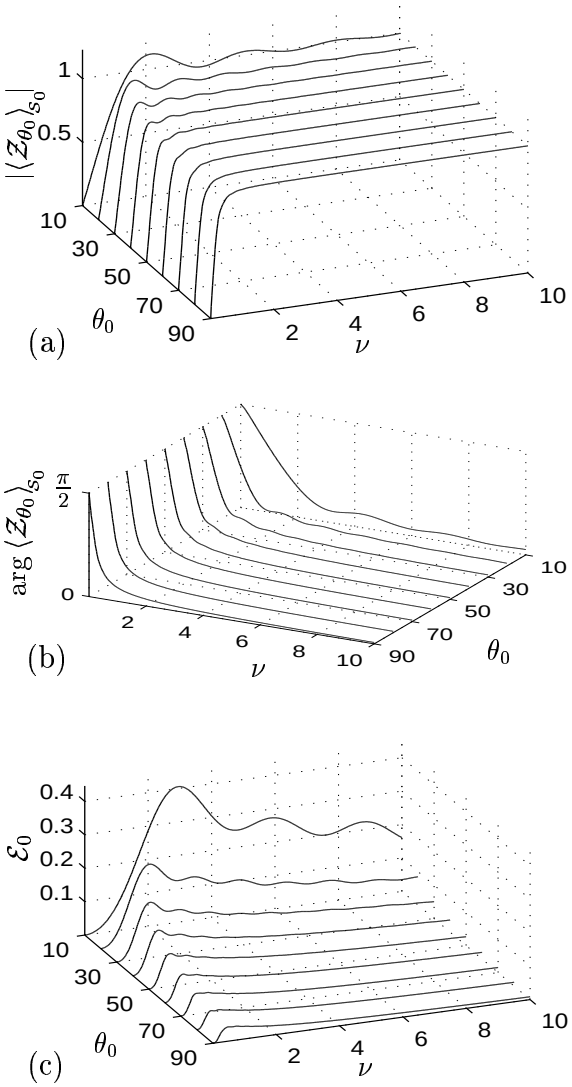

Figure 3: Computation of the averaged normalized specific impedance $\langle \mathcal{Z}_{\theta_0} \rangle_{S_0}$ in the frequency domain for the first modes ($N = 300$) and for $10° \leq \theta_0 \leq 90°$ and $0 \leq \nu \leq 10$. (a) Modulus of $\langle \mathcal{Z}_{\theta_0} \rangle_{S_0}$. (b) Phase of $\langle \mathcal{Z}_{\theta_0} \rangle_{S_0}$. (c) Mean square error $\mathcal{E}_0$ due to the averaging.

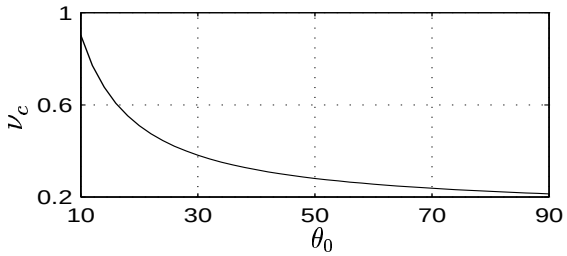

Figure 4: Optimal parameter values $\nu_c(\theta_0)$ obtained for $\mathcal{M}_1$.

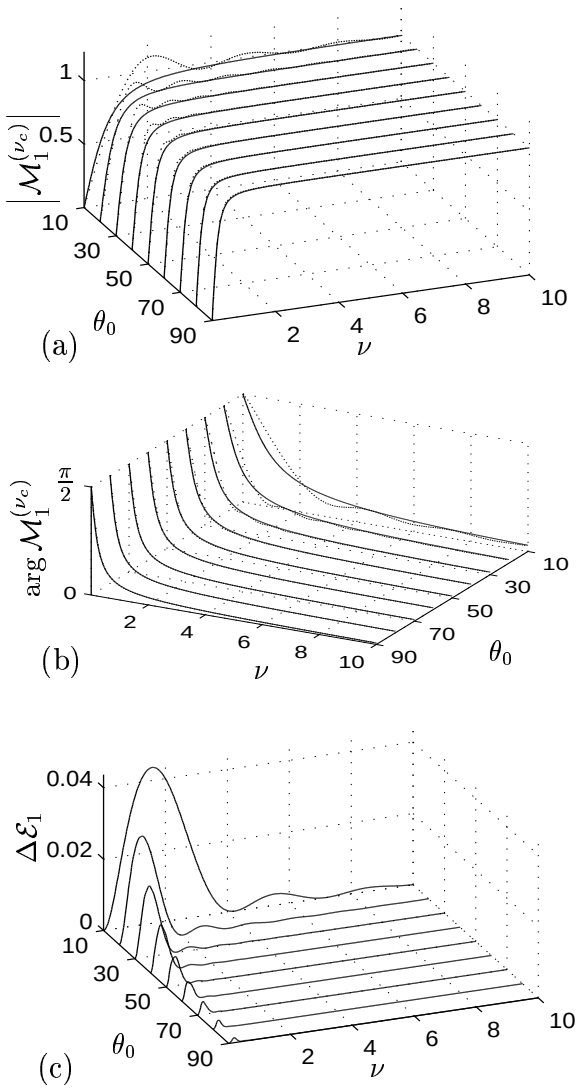

Figure 5: Comparative layouts of $\mathcal{M}_1^{(\nu_c)}$ $(-)$ and $\langle \mathcal{Z}_{\theta_0} \rangle_{S_0}$ $(...)$ for: (a) the modulus, (b) the phase. (c) Square error $\Delta\mathcal{E}_1$ due to the approximation of $\langle \mathcal{Z}_{\theta_0} \rangle_{S_0}$ by $\mathcal{M}_1^{(\nu_c)}$.

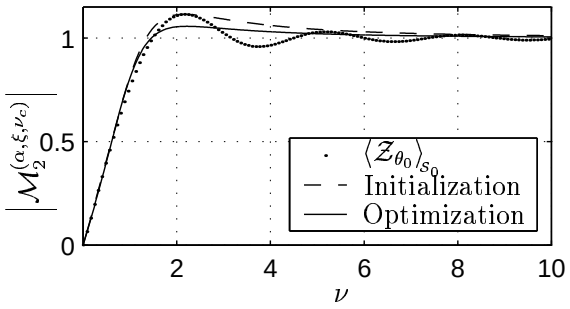

Figure 6: Local optimization of the parameter values of $\mathcal{M}_2$ for $\theta_0 = 10°$: modulus of $\mathcal{M}_2$ obtained for initialization parameters (- -), modulus of $\mathcal{M}_2$ obtained for optimized parameters $(-)$, and reference $|\langle \mathcal{Z}_{\theta_0} \rangle_{S_0}|$ (...).

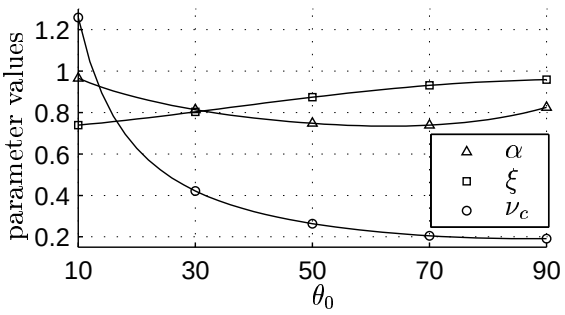

Figure 7: Optimal parameter values $\alpha(\theta_0)$, $\xi(\theta_0)$, and $\nu_c(\theta_0)$, obtained for $\mathcal{M}_2$.

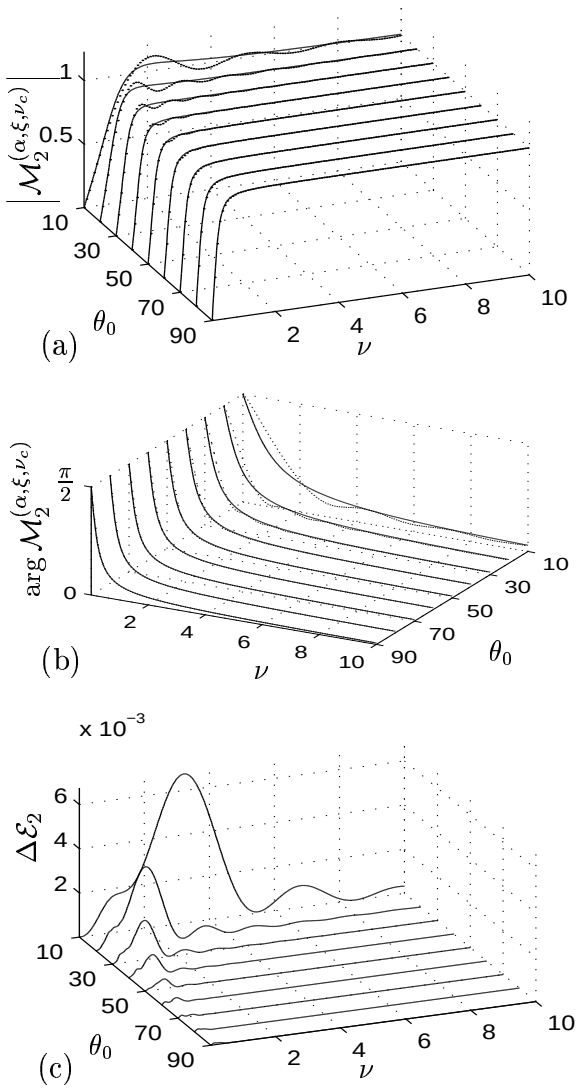

Figure 8: Comparative layouts of $\mathcal{M}_2^{(\alpha,\xi,\nu_c)}$ $(-)$ and $\langle \mathcal{Z}_{\theta_0} \rangle_{S_0}$ $(...)$ for: (a) the modulus, (b) the phase. (c) Square error $\Delta\mathcal{E}_2$ due to the approximation of $\langle \mathcal{Z}_{\theta_0} \rangle_{S_0}$ by $\mathcal{M}_2^{(\alpha,\xi,\nu_c)}$.

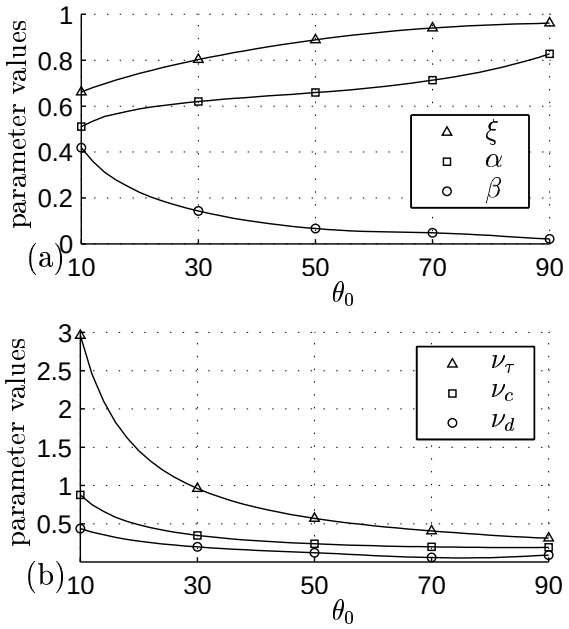

Figure 9: Optimal parameter values obtained for $\mathcal{M}_3$. (a): $\alpha(\theta_0)$, $\xi(\theta_0)$, $\beta(\theta_0)$. (b): $\nu_c(\theta_0)$, $\nu_\tau(\theta_0)$ and $\nu_d(\theta_0)$.

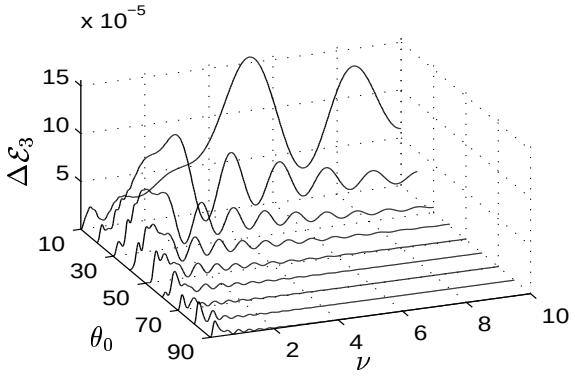

Figure 10: Square error $\Delta\mathcal{E}_3$ due to the approximation of $\langle\mathcal{Z}_{\theta_0}\rangle_{S_0}$ by $\mathcal{M}_3^{(\alpha,\xi,\nu_c,\beta,\nu_\tau,\nu_d)}$.

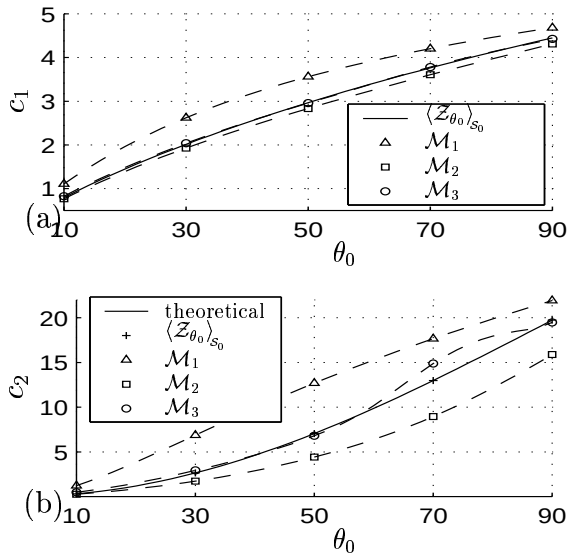

Figure 11: Coefficients c_1 (a) and c_2 (b) of the series expansion of $\langle \mathcal{Z}_{\theta_0} \rangle_{S_0}(\nu)$ and $\mathcal{M}_{k=1,2,3}(\nu)$ defined in Eq. (37).

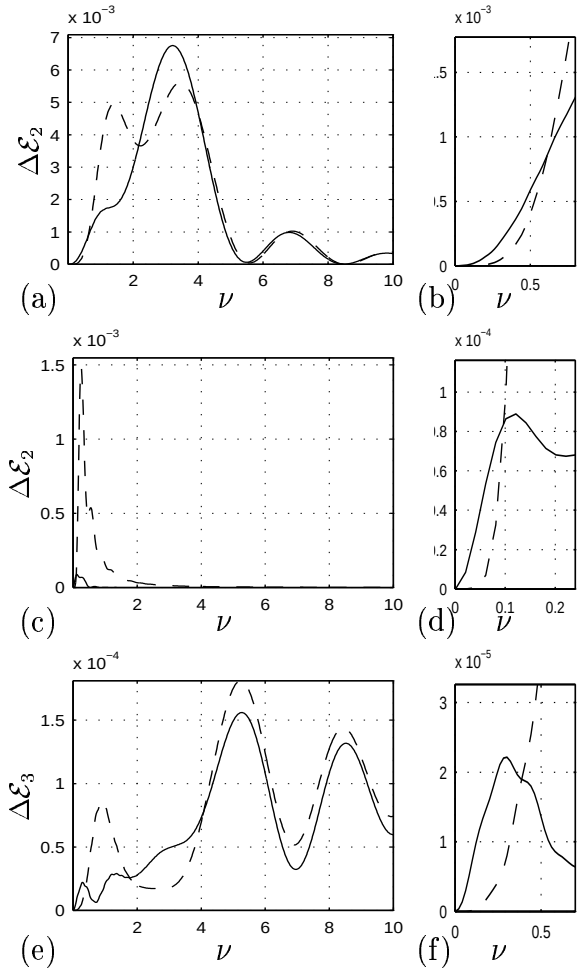

Figure 12: Error $\Delta\mathcal{E}_{k=2,3}$ measured on $\mathcal{M}_{k=2,3}$ for optimal parameters with constraints (- -), and without constraints (-). (a) Errors for $k = 2$, $\theta_0 = 10°$ on the complete frequency range. (b) Errors for $k = 2$, $\theta_0 = 10°$ in the low frequency range (zoom). (c) Errors for $k = 2$, $\theta_0 = 90°$ on the complete frequency range. (d) Errors for $k = 2$, $\theta_0 = 90°$ in the low frequency range (zoom). (e) Errors for $k = 3$, $\theta_0 = 10°$ on the complete frequency range. (f) Errors for $k = 3$, $\theta_0 = 10°$ in the low frequency range (zoom).

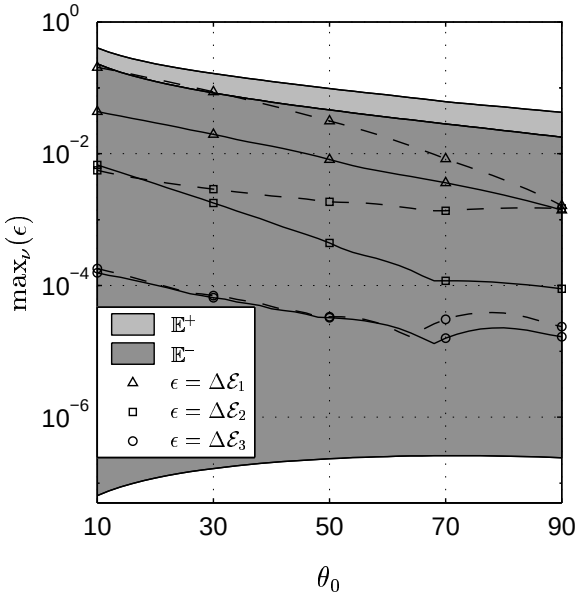

Figure 13: Comparison of the error $\mathcal{E}_0$ introduced by the averaging operator $\langle . \rangle_{S_0}$ with the ν-maximal added errors $\Delta\mathcal{E}_{k=1,2,3}$ due to the approximation of $\langle \mathcal{Z}_{\theta_0} \rangle_{S_0}$ by $\mathcal{M}_{k=1,2,3}$. Results are given for the optimal paramters with constraints (- -) and without constraints (- -). $\mathbb{E}^+$ and $\mathbb{E}^-$ are defined by

$$\mathbb{E}^+ \triangleq \left\{ (\theta_0, \epsilon) \,/\, \max_\nu \left(\mathcal{E}_0(\theta_0,\nu)\right) \geq \epsilon \geq \operatorname*{mean}_\nu \left(\mathcal{E}_0(\theta_0,\nu)\right) \right\}, \text{ and}$$

$$\mathbb{E}^- \triangleq \left\{ (\theta_0, \epsilon) \,/\, \operatorname*{mean}_\nu \left(\mathcal{E}_0\left(\theta_0,\nu\right)\right) \geq \epsilon \geq \min_\nu \left(\mathcal{E}_0(\theta_0,\nu)\right) \right\}$$

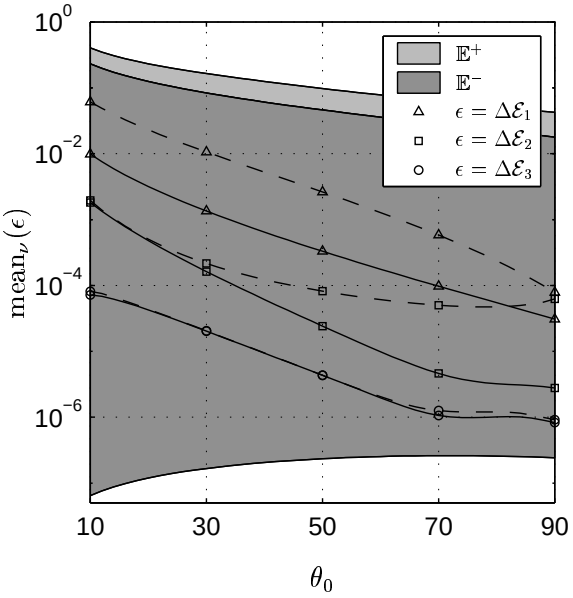

Figure 14: Comparison of the error $\mathcal{E}_0$ introduced by the averaging operator $\langle . \rangle_{S_0}$ with the ν-averaged added errors $\Delta\mathcal{E}_{k=1,2,3}$ due to the approximation of $\langle \mathcal{Z}_{\theta_0} \rangle_{S_0}$ by $\mathcal{M}_{k=1,2,3}$. Results are given for the optimal paramters with constraints (- -) and without constraints (- -).

	c_1	c_2
$\mathcal{M}_1$	$\frac{1}{\nu_c}$	$\frac{1}{{\nu_c}^2}$
$\mathcal{M}_2$	$\frac{\alpha}{\nu_c}$	$\frac{2\alpha\xi-1}{{\nu_c}^2}$
$\mathcal{M}_3$	$(1+\beta)\frac{\alpha}{\nu_c}$	$(1+\beta)\frac{2\alpha\xi-1}{{\nu_c}^2}$ $+\frac{\alpha\beta}{\nu_c}\left(\frac{2\pi}{\nu_\tau}+\frac{1}{\nu_d}\right)$

Table I: Coefficients of the series expansion of $\mathcal{M}_{k=1,2,3}$.

	$\mathcal{M}_1$	$\mathcal{M}_2$	$\mathcal{M}_3$
A_0	1	1	1
A_1	$1/\omega_c$	$2\xi/\omega_c$	$2\xi/\omega_c + 1/\omega_d$
A_2	0	1	$1/{\omega_c}^2 + 2\xi/(\omega_c\omega_d)$
A_3	0	0	$1/({\omega_c}^2\omega_d)$
B_1	$1/\omega_c$	α/ω_c	α/ω_c
B_2	0	1	$1/{\omega_c}^2 + \alpha/(\omega_c\omega_d)$
B_3	0	0	$1/({\omega_c}^2\omega_d)$
C_1	0	0	$\alpha\beta/\omega_c$
C_2	0	0	$\beta/{\omega_c}^2$

Table II: Coefficients of the dynamical systems associated with $\mathcal{M}_{k=1,2,3}$.

Monomials	X^5	X^4	X^3	X^2	X^1	X^0
$\mathcal{P}_\alpha$	0.1113	-0.6360	1.162	-1.242	1.083	0.8788
$\mathcal{P}_\xi$	0	0.0207	-0.144	0.221	0.0799	0.720
$\mathcal{P}_{\nu_c}$	-0.1980	0.2607	-0.4240	-0.07946	4.704	-0.0220

Table III: Coefficients of the polynomials used to model the parameters α, ξ, and ν_c. These parameters are functions of θ_0 and used in $\mathcal{M}_2$.

θ_0	α	ξ	ν_c	β	ν_τ	ν_d
10°	$5.108\,10^{-1}$	$6.619\,10^{-1}$	$8.776\,10^{-1}$	$4.191\,10^{-1}$	2.959	$4.377\,10^{-1}$
12°	$5.348\,10^{-1}$	$6.809\,10^{-1}$	$7.503\,10^{-1}$	$3.592\,10^{-1}$	2.455	$3.903\,10^{-1}$
14°	$5.549\,10^{-1}$	$6.980\,10^{-1}$	$6.585\,10^{-1}$	$3.119\,10^{-1}$	2.095	$3.546\,10^{-1}$
16°	$5.671\,10^{-1}$	$7.140\,10^{-1}$	$5.864\,10^{-1}$	$2.775\,10^{-1}$	1.827	$3.223\,10^{-1}$
18°	$5.777\,10^{-1}$	$7.289\,10^{-1}$	$5.300\,10^{-1}$	$2.493\,10^{-1}$	1.619	$2.950\,10^{-1}$
20°	$5.885\,10^{-1}$	$7.427\,10^{-1}$	$4.854\,10^{-1}$	$2.243\,10^{-1}$	1.453	$2.731\,10^{-1}$
22°	$5.964\,10^{-1}$	$7.559\,10^{-1}$	$4.481\,10^{-1}$	$2.035\,10^{-1}$	1.318	$2.538\,10^{-1}$
24°	$6.026\,10^{-1}$	$7.685\,10^{-1}$	$4.165\,10^{-1}$	$1.858\,10^{-1}$	1.205	$2.364\,10^{-1}$
26°	$6.093\,10^{-1}$	$7.804\,10^{-1}$	$3.902\,10^{-1}$	$1.699\,10^{-1}$	1.111	$2.215\,10^{-1}$
28°	$6.152\,10^{-1}$	$7.917\,10^{-1}$	$3.675\,10^{-1}$	$1.556\,10^{-1}$	1.030	$2.085\,10^{-1}$
30°	$6.199\,10^{-1}$	$8.026\,10^{-1}$	$3.476\,10^{-1}$	$1.431\,10^{-1}$	$9.594\,10^{-1}$	$1.966\,10^{-1}$
32°	$6.246\,10^{-1}$	$8.130\,10^{-1}$	$3.302\,10^{-1}$	$1.318\,10^{-1}$	$8.982\,10^{-1}$	$1.860\,10^{-1}$
34°	$6.293\,10^{-1}$	$8.228\,10^{-1}$	$3.151\,10^{-1}$	$1.214\,10^{-1}$	$8.442\,10^{-1}$	$1.765\,10^{-1}$
36°	$6.333\,10^{-1}$	$8.324\,10^{-1}$	$3.015\,10^{-1}$	$1.119\,10^{-1}$	$7.963\,10^{-1}$	$1.680\,10^{-1}$
38°	$6.371\,10^{-1}$	$8.415\,10^{-1}$	$2.893\,10^{-1}$	$1.034\,10^{-1}$	$7.536\,10^{-1}$	$1.601\,10^{-1}$
40°	$6.410\,10^{-1}$	$8.502\,10^{-1}$	$2.785\,10^{-1}$	$9.561\,10^{-2}$	$7.152\,10^{-1}$	$1.528\,10^{-1}$
42°	$6.447\,10^{-1}$	$8.586\,10^{-1}$	$2.687\,10^{-1}$	$8.849\,10^{-2}$	$6.805\,10^{-1}$	$1.461\,10^{-1}$
44°	$6.482\,10^{-1}$	$8.666\,10^{-1}$	$2.598\,10^{-1}$	$8.208\,10^{-2}$	$6.490\,10^{-1}$	$1.396\,10^{-1}$
46°	$6.517\,10^{-1}$	$8.743\,10^{-1}$	$2.517\,10^{-1}$	$7.630\,10^{-2}$	$6.203\,10^{-1}$	$1.334\,10^{-1}$
48°	$6.554\,10^{-1}$	$8.816\,10^{-1}$	$2.444\,10^{-1}$	$7.115\,10^{-2}$	$5.941\,10^{-1}$	$1.271\,10^{-1}$
50°	$6.590\,10^{-1}$	$8.887\,10^{-1}$	$2.377\,10^{-1}$	$6.666\,10^{-2}$	$5.701\,10^{-1}$	$1.207\,10^{-1}$
52°	$6.627\,10^{-1}$	$8.954\,10^{-1}$	$2.316\,10^{-1}$	$6.279\,10^{-2}$	$5.479\,10^{-1}$	$1.141\,10^{-1}$
54°	$6.668\,10^{-1}$	$9.018\,10^{-1}$	$2.260\,10^{-1}$	$5.957\,10^{-2}$	$5.275\,10^{-1}$	$1.072\,10^{-1}$
56°	$6.711\,10^{-1}$	$9.078\,10^{-1}$	$2.210\,10^{-1}$	$5.705\,10^{-2}$	$5.087\,10^{-1}$	$9.975\,10^{-2}$
58°	$6.757\,10^{-1}$	$9.135\,10^{-1}$	$2.164\,10^{-1}$	$5.513\,10^{-2}$	$4.912\,10^{-1}$	$9.215\,10^{-2}$
60°	$6.809\,10^{-1}$	$9.189\,10^{-1}$	$2.124\,10^{-1}$	$5.367\,10^{-2}$	$4.748\,10^{-1}$	$8.461\,10^{-2}$
62°	$6.865\,10^{-1}$	$9.238\,10^{-1}$	$2.087\,10^{-1}$	$5.263\,10^{-2}$	$4.596\,10^{-1}$	$7.732\,10^{-2}$
64°	$6.924\,10^{-1}$	$9.285\,10^{-1}$	$2.054\,10^{-1}$	$5.175\,10^{-2}$	$4.452\,10^{-1}$	$7.078\,10^{-2}$
...	...	...	...	...	...	...

θ_0	α	ξ	ν_c	β	ν_τ	ν_d
66°	$6.988\,10^{-1}$	$9.328\,10^{-1}$	$2.024\,10^{-1}$	$5.074\,10^{-2}$	$4.316\,10^{-1}$	$6.530\,10^{-2}$
68°	$7.056\,10^{-1}$	$9.367\,10^{-1}$	$1.998\,10^{-1}$	$4.960\,10^{-2}$	$4.186\,10^{-1}$	$6.081\,10^{-2}$
70°	$7.128\,10^{-1}$	$9.403\,10^{-1}$	$1.975\,10^{-1}$	$4.823\,10^{-2}$	$4.063\,10^{-1}$	$5.734\,10^{-2}$
72°	$7.204\,10^{-1}$	$9.437\,10^{-1}$	$1.955\,10^{-1}$	$4.651\,10^{-2}$	$3.945\,10^{-1}$	$5.501\,10^{-2}$
74°	$7.288\,10^{-1}$	$9.467\,10^{-1}$	$1.937\,10^{-1}$	$4.443\,10^{-2}$	$3.830\,10^{-1}$	$5.377\,10^{-2}$
76°	$7.378\,10^{-1}$	$9.494\,10^{-1}$	$1.923\,10^{-1}$	$4.209\,10^{-2}$	$3.720\,10^{-1}$	$5.356\,10^{-2}$
78°	$7.476\,10^{-1}$	$9.518\,10^{-1}$	$1.912\,10^{-1}$	$3.951\,10^{-2}$	$3.615\,10^{-1}$	$5.448\,10^{-2}$
80°	$7.583\,10^{-1}$	$9.539\,10^{-1}$	$1.904\,10^{-1}$	$3.664\,10^{-2}$	$3.513\,10^{-1}$	$5.680\,10^{-2}$
82°	$7.700\,10^{-1}$	$9.558\,10^{-1}$	$1.899\,10^{-1}$	$3.350\,10^{-2}$	$3.414\,10^{-1}$	$6.082\,10^{-2}$
84°	$7.829\,10^{-1}$	$9.574\,10^{-1}$	$1.898\,10^{-1}$	$3.018\,10^{-2}$	$3.321\,10^{-1}$	$6.690\,10^{-2}$
86°	$7.967\,10^{-1}$	$9.588\,10^{-1}$	$1.899\,10^{-1}$	$2.685\,10^{-2}$	$3.236\,10^{-1}$	$7.524\,10^{-2}$
88°	$8.115\,10^{-1}$	$9.601\,10^{-1}$	$1.904\,10^{-1}$	$2.388\,10^{-2}$	$3.171\,10^{-1}$	$8.473\,10^{-2}$
90°	$8.274\,10^{-1}$	$9.613\,10^{-1}$	$1.911\,10^{-1}$	$2.189\,10^{-2}$	$3.141\,10^{-1}$	$9.101\,10^{-2}$

Table IV: Optimal parameters values α, ξ, ν_c, β, ν_τ, and ν_d. These parameters are functions of θ_0 and used in $\mathcal{M}_3$.

x	$-\infty$		x^*		$+\infty$
$f(x)$	0	$\searrow$	f^*	$\nearrow$	$+\infty$

Table V: Variational study of the function $x \mapsto f(x)$ defined by Eq. (C3)

LIST OF LEGENDS

Figure 1 *The radiation of the horn is approximated by that of the sphere $\mathcal{S}$, part of which, $\mathcal{S}_0$, is pulsating with an uniform velocity while the other remains motionless. The radius of $\mathcal{S}$ is noted r_0, and the angle of the tangent cone at the horn output is noted θ_0.*

Figure 2 *Approximation of the normalized velocity $V_{\mathcal{S}}/v_0$ and the modulus of the normalized pressure in the frequency domain $p_{\mathcal{S}}/(Z_c v_0)$, both computed for the first modes ($N = 300$). (a) Normalized velocity calulated with $\theta_0 = 30°$. (b) Normalized velocity calulated with $\theta = 70°$. (c) Normalized pressure calulated with $\theta = 30°$. (d) Normalized pressure calulated with $\theta = 70°$.*

Figure 3 *Computation of the averaged normalized specific impedance $\langle \mathcal{Z}_{\theta_0} \rangle_{\mathcal{S}_0}$ in the frequency domain for the first modes ($N=300$) and for $10° \leq \theta_0 \leq 90°$ and $0 \leq \nu \leq 10$. (a) Modulus of $\langle \mathcal{Z}_{\theta_0} \rangle_{\mathcal{S}_0}$. (b) Phase of $\langle \mathcal{Z}_{\theta_0} \rangle_{\mathcal{S}_0}$. (c) Mean square error $\mathcal{E}_0$ due to the averaging.*

Figure 4 *Optimal parameter values $\nu_c(\theta_0)$ obtained for $\mathcal{M}_1$.*

Figure 5 *Comparative layouts of $\mathcal{M}_1^{(\nu_c)}$ (−) and $\langle \mathcal{Z}_{\theta_0} \rangle_{\mathcal{S}_0}$ (...) for: (a) the modulus, (b) the phase. (c) Square error $\Delta\mathcal{E}_1$ due to the approximation of $\langle \mathcal{Z}_{\theta_0} \rangle_{\mathcal{S}_0}$ by $\mathcal{M}_1^{(\nu_c)}$.*

Figure 6 *Local optimization of the parameter values of $\mathcal{M}_2$ for $\theta_0 = 10°$: modulus of $\mathcal{M}_2$ obtained for initialization parameters (- -), modulus of $\mathcal{M}_2$ obtained for optimized parameters (−), and reference $|\langle \mathcal{Z}_{\theta_0} \rangle_{\mathcal{S}_0}|$ (...).*

Figure 7 *Optimal parameter values $\alpha(\theta_0)$, $\xi(\theta_0)$, and $\nu_c(\theta_0)$, obtained for $\mathcal{M}_2$.*

Figure 8 *Comparative layouts of $\mathcal{M}_2^{(\alpha,\xi,\nu_c)}$ (−) and $\langle \mathcal{Z}_{\theta_0} \rangle_{\mathcal{S}_0}$ (...) for: (a) the modulus, (b) the phase. (c) Square error $\Delta\mathcal{E}_2$ due to the approximation of $\langle \mathcal{Z}_{\theta_0} \rangle_{\mathcal{S}_0}$ by $\mathcal{M}_2^{(\alpha,\xi,\nu_c)}$.*

Figure 9 *Optimal parameter values obtained for $\mathcal{M}_3$. (a): $\alpha(\theta_0)$, $\xi(\theta_0)$, $\beta(\theta_0)$. (b): $\nu_c(\theta_0)$, $\nu_\tau(\theta_0)$ and $\nu_d(\theta_0)$.*

Figure 10 *Square error $\Delta\mathcal{E}_3$ due to the approximation of $\langle\mathcal{Z}_{\theta_0}\rangle_{S_0}$ by $\mathcal{M}_3^{(\alpha,\xi,\nu_c,\beta,\nu_\tau,\nu_d)}$.*

Figure 11 *Coefficients c_1 (a) and c_2 (b) of the series expansion of $\langle\mathcal{Z}_{\theta_0}\rangle_{S_0}(\nu)$ and $\mathcal{M}_{k=1,2,3}(\nu)$ defined in Eq. (37).*

Figure 12 *Error $\Delta\mathcal{E}_{k=2,3}$ measured on $\mathcal{M}_{k=2,3}$ for optimal parameters with constraints (- -), and without constraints (-). (a) Errors for $k=2$, $\theta_0=10°$ on the complete frequency range. (b) Errors for $k=2$, $\theta_0=10°$ in the low frequency range (zoom). (c) Errors for $k=2$, $\theta_0=90°$ on the complete frequency range. (d) Errors for $k=2$, $\theta_0=90°$ in the low frequency range (zoom). (e) Errors for $k=3$, $\theta_0=10°$ on the complete frequency range. (f) Errors for $k=3$, $\theta_0=10°$ in the low frequency range (zoom).*

Figure 13 *Comparison of the error $\mathcal{E}_0$ introduced by the averaging operator $\langle.\rangle_{S_0}$ with the ν-maximal added errors $\Delta\mathcal{E}_{k=1,2,3}$ due to the approximation of $\langle\mathcal{Z}_{\theta_0}\rangle_{S_0}$ by $\mathcal{M}_{k=1,2,3}$. Results are given for the optimal paramters with constraints (- -) and without constraints (- -). $\mathbb{E}^+$ and $\mathbb{E}^-$ are defined by*

$$\mathbb{E}^+ \triangleq \left\{(\theta_0,\epsilon)\,/\ \max_{\nu}\ (\mathcal{E}_0(\theta_0,\nu)) \geq \epsilon \geq \operatorname*{mean}_{\nu}\ (\mathcal{E}_0(\theta_0,\nu))\right\}, \text{ and}$$

$$\mathbb{E}^- \triangleq \left\{(\theta_0,\epsilon)\,/\ \operatorname*{mean}_{\nu}\ (\mathcal{E}_0(\theta_0,\nu)) \geq \epsilon \geq \min_{\nu}\ (\mathcal{E}_0(\theta_0,\nu))\right\}$$

Figure 14 *Comparison of the error $\mathcal{E}_0$ introduced by the averaging operator $\langle.\rangle_{S_0}$ with the ν-averaged added errors $\Delta\mathcal{E}_{k=1,2,3}$ due to the approximation of $\langle\mathcal{Z}_{\theta_0}\rangle_{S_0}$ by $\mathcal{M}_{k=1,2,3}$. Results are given for the optimal paramters with constraints (- -) and without constraints (- -).*

Table I *Coefficients of the series expansion of $\mathcal{M}_{k=1,2,3}$.*

Table II *Coefficients of the dynamical systems associated with $\mathcal{M}_{k=1,2,3}$.*

Table III *Coefficients of the polynomials used to model the parameters α, ξ, and ν_c. These parameters are functions of θ_0 and used in $\mathcal{M}_2$.*

Table IV *Optimal parameters values* α, ξ, ν_c, β, ν_τ, *and* ν_d. *These parameters are functions of* θ_0 *and used in* $\mathcal{M}_3$.

Table V *Variational study of the function* $x \mapsto f(x)$ *defined by Eq. (C3)*